Heliyon 11 (2025) e41979

Contents lists available at ScienceDirect

Heliyon

journal homepage: www.cell.com/heliyon

Research article

Mouse ZGRF1 helicase facilitates DNA repair and maintains efficient fertility

Ernest Wee Kiat Lim [a,b], Smaragda Kompocholi [a], André Brannvoll [a,b,e], K. Stine V. Bagge [a,f], Jennifer R. Gruhn [b], Javier Martin-Gonzalez [c], Eliene Albers [b], Ian D. Hickson [b], Andrés López-Contreras [b,d], Michael Lisby [a,b,*]

[a] Section for Functional Genomics, Department of Biology University of Copenhagen, 2200, Copenhagen N, Denmark
[b] Center for Chromosome Stability, Department of Cellular and Molecular Medicine, University of Copenhagen, 2200, Copenhagen N, Denmark
[c] Core Facility for Transgenic Mice, Department of Experimental Medicine, University of Copenhagen, 2200, Copenhagen N, Denmark
[d] Centro Andaluz de Biología Molecular y Medicina Regenerativa (CABIMER), Consejo Superior de Investigaciones Científicas (CSIC), Universidad de Sevilla - Universidad Pablo de Olavide, Seville, Spain
[e] Høiberg P/S, Adelgade 12, 1304, Copenhagen K, Denmark
[f] Emendo Research & Development, 2150, Nordhavn, Denmark

ARTICLE INFO

Keywords:
ZGRF1
DNA helicase
Interstrand crosslinks
DNA repair
Homologous recombination
Mouse model

ABSTRACT

The recently characterised human ZGRF1 helicase promotes genomic stability by facilitating DNA interstrand crosslink repair. In its absence, human cells exhibit greater sensitivity towards anti-cancer drugs such as mitomycin C and camptothecin. Moreover, the downregulation of *ZGRF1* expression is associated with increased survival in cancer patients. These attributes point to ZGRF1 as a potential anti-cancer drug target. Here, we investigated the role of ZGRF1 in tumorigenesis using the mouse model. We generated a ZGRF1 mutant mouse and find that it is viable and displays normal development. However, at a cellular level, mouse embryonic fibroblasts exhibit sensitivity to ICLs and show elevated levels of the DNA damage marker γH2AX. In the absence of ZGRF1, the rates of tumorigenesis and tumour-free survival in Eμ-*Myc* and *Trp53* knockout mice remained largely unaffected. These findings suggest a potential role for ZGRF1 in the proliferation of specific cancer types, highlighting avenues for further research in other cancer models. Additionally, beyond its known function in DNA repair, our study also reveals that ZGRF1 promotes meiotic recombination and that its loss results in reduced fertility in mice manifested as a 30 % reduction in meiotic crossovers and a 15 % reduction in litter size.

1. Introduction

The significance of DNA repair mechanisms is underscored by their critical role in the maintenance of genome integrity [1]. The human genome is constantly exposed to physical and chemical agents that can induce DNA lesions [2]. When lesions are not promptly

Abbreviations: ADH5, Alcohol dehydrogenase 5; CPT, Camptothecin; Dbl2, DNA-break-localising 2 protein; DDR, DNA damage response; DSB, DNA double-strand break; DUF, Domain of unknown function; FA, Fanconi Anaemia; HR, Homologous recombination; ICL, Interstrand crosslink; MEFs, Mouse embryonic fibroblasts; MMC, Mitomycin C; ZGRF1, Zinc finger GRF-type containing 1.

* Corresponding author. Section for Functional Genomics, Department of Biology University of Copenhagen, 2200, Copenhagen N, Denmark.
E-mail address: mlisby@bio.ku.dk (M. Lisby).

https://doi.org/10.1016/j.heliyon.2025.e41979
Received 23 September 2024; Received in revised form 13 January 2025; Accepted 14 January 2025
Available online 16 January 2025

and properly repaired, they can cause mutations and replication stress, resulting in genomic instability. As one of the foremost enabling characteristics of cancer, genome instability compromises surveillance and repair systems, enabling cells to evade senescence and apoptosis. This paves the way for neoplastic transformation and the eventual development of tumours [3]. Understanding genomic instability is crucial for deciphering the mechanisms that drive the survival, proliferation, and metastasis of cancer cells. Moreover, the mechanisms safeguarding the genome offer potential avenues for the development of anti-cancer therapeutics to eradicate malignant cells [4].

DNA double-strand breaks (DSBs) constitute one of the most severe types of DNA damage and can lead to the detachment of chromosome fragments from their centromeres. DSBs can occur at a rate as high as 50 per day in each cell [5], and aberrant rearrangements can result if breaks are repaired sub-optimally [6]. On the other hand, if left unrepaired, DSBs can result in the loss of genetic information, as fragments lacking a centromere may fail to segregate during cell division [7]. DSBs can arise through replication stress, as an intermediate during repair processes, or be induced by endogenous and exogenous sources such as the meiosis-specific endonuclease SPO11, reactive oxygen species (ROS) or ionising radiation (IR) [8,9]. To mitigate chromosomal rearrangements and the loss of genetic information, cells have evolved an essentially error-free pathway, homologous recombination (HR), to faithfully repair DSBs.

In HR, an undamaged copy of DNA, typically the sister chromatid, is used as the repair template to restore the damaged strand. The initiation of HR involves end-resection, generating 3′ single-stranded DNA (ssDNA) tails that enable homology search by the RAD51 recombinase and the subsequent process of strand invasion. Using the undamaged sister chromatid as the repair template, the 3′ end primes DNA synthesis to restore genetic information at the DSB. HR is also utilised in the Fanconi Anaemia (FA) pathway, as evidenced by its requirement for HR factors such as RAD51 and the BRCA1 tumour suppressor. In response to repair of replication-blocking DNA interstrand crosslinks (ICLs), the FA core complex is assembled at the ICL-replisome. Subsequently, the FANCI-FANCD2 (ID2) heterodimer is recruited and monoubiquitylated to mediate the excision of one of the two covalently crosslinked nucleotides. This process, known as unhooking, generates two intermediates: a partially replicated parental strand that continues to harbour the ICL adduct, and a DSB. While the first intermediate is repaired via the translesion synthesis and nucleotide excision repair pathways, the DSB is repaired by HR [10]. Both RAD51 and BRCA1 interact with the ICL-replisome before unhooking. RAD51 binds to the ssDNA region to protect the fork from degradation, while ID2 recruits BRCA1 to evict the replicative helicase before the ICL is unhooked [11,12]. Subsequently, BRCA1 recruits BRCA2 to catalyse RPA–RAD51 exchange on the 3′ ssDNA tail, enabling RAD51 to carry out the homology search and facilitate strand invasion [13,14]. The crosstalk between the components of the two pathways, along with the association of mutations in these HR factors in FA patients, indicates an intricate role of HR in the FA pathway [15–17].

DNA helicases play a crucial role in unwinding duplex DNA to facilitate various cellular processes such as replication and repair. Their indispensable functions extend to both the FA and HR pathways, where they can disrupt complex DNA secondary structures, displace proteins bound to ssDNA, promote strand annealing, dissociate D-loops, facilitate branch migration, and dissolve double Holliday Junctions (dHJs) [18]. One notable helicase involved in both of these repair pathways is ZGRF1 (Zinc finger GRF-type containing 1), which besides a highly conserved N-terminal domain of unknown function 2439 (DUF2439) has an central Zn-finger motif and a C-terminal helicase domain with 5′ to 3′ DNA helicase activity (Fig. 1a) [19]. ZGRF1 plays a pivotal role in the repair of ICLs by physically interacting with RAD51 to stimulate RAD51-RAD54-mediated strand exchange. ZGRF1 may also play a role in the subsequent steps of D-loop dissociation and HJ branch migration, promoting crossover formation [19]. Cells lacking ZGRF1 are sensitive to mitomycin C (MMC), a DNA crosslinking agent, and camptothecin, a topoisomerase I poison. In its absence, both FANCD2 and RAD51 foci accumulate at DSBs, while cell cycle arrest occurs at the G2 phase. Additionally, MMC-treated *ZGRF1*$^{-/-}$ cells accumulate chromosomal aberrations and exhibit a reduction in sister chromatid exchange (SCE). Based on these findings, it was suggested that while ZGRF1 is not required for the activation of the FA pathway, it is recruited downstream of ID2 monoubiquitylation to facilitate HR. In the absence of ZGRF1, DSBs induced during the processing of ICLs might be sub-optimally repaired, leading to genomic instability [19].

Presently, there are no reports of mutations in *ZGRF1* associated with cancer or FA. However, ZGRF1 variants have been linked to several phenotypes in humans, including obesity, childhood apraxia of speech, hot water epilepsy and reduced overall survival of triple-negative breast cancer patients [20–24]. In this study, we generated a *Zgrf1* mutant mouse to study the role of ZGRF1 in the maintenance of genome stability *in vivo* and in combination with two well-characterised cancer models, the Eμ-*Myc* and *Trp53* KO mice to assess the impact of ZGRF1 mutation on tumorigenesis and survival [25,26]. First, we showed that the mutation of ZGRF1 did not affect the development and viability of mice, although at a cellular level mouse embryonic fibroblasts were sensitive to ICLs. We also demonstrated that the mutation of ZGRF1 does not promote tumorigenesis in Eμ-*Myc* and *Trp53* KO models. However, our data suggest that ZGRF1 could facilitate the loss of heterozygosity that accelerates tumorigenesis in *Trp53*$^{+/-}$ heterozygous (het) mice. Finally, since ZGRF1 promotes the formation of mitotic crossovers and its fission yeast homolog Dbl2 (*Schizosaccharomyces pombe*) is required for proper meiotic chromosome segregation, we examined if ZGRF1 is involved in gametogenesis in mice [27]. Through fertility studies and the examination of spermatocytes from the *Zgrf1* KO mice, we established that ZGRF1 can also facilitate the formation of crossovers during meiosis.

2. Results

2.1. Generation of the Zgrf1 mutant mouse

Utilising the CRISPR-Cas9 gene editing technique, a 5-base pair deletion was introduced in exon 4 of the *Zgrf1* gene. This allele is designated *Zgrf1*^{em1Ucph} and will be referred to as *Zgrf1*^{mut} hereafter. This frameshift mutation results in a stop codon that terminates

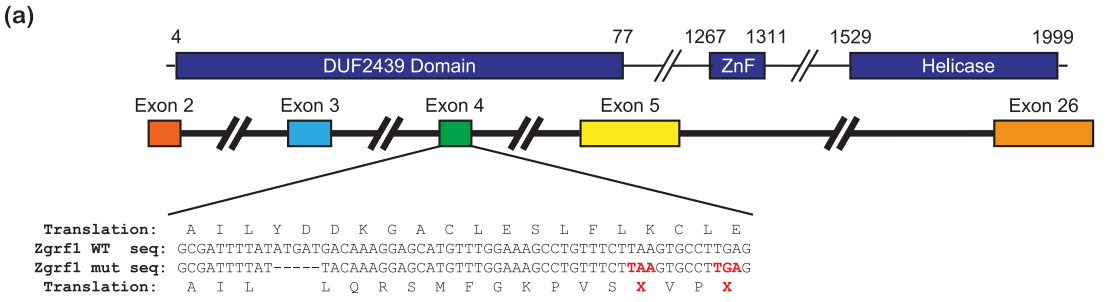

(b)

Cross: *Zgrf1* $^{+/mut}$ x *Zgrf1* $^{+/mut}$					
Genotype	**Observed**	**Value**	**Expected**	**Freq. observed (%)**	**Freq. expected (%)**
Zgrf1 $^{mut/mut}$	115	Low	129.75	22.16	25
Zgrf1 $^{+/mut}$	274	High	259.5	52.79	50
Zgrf1 $^{+/+}$	130	High	129.75	25.05	25
Total	519		519	100	100
	Chi-square calculated value:			2.487	MENDELIAN
	Chi-square table:			5.991	
	Confidence level:			0.05	
	Calculated p-value:			0.288	
	Degrees of freedom:			2	

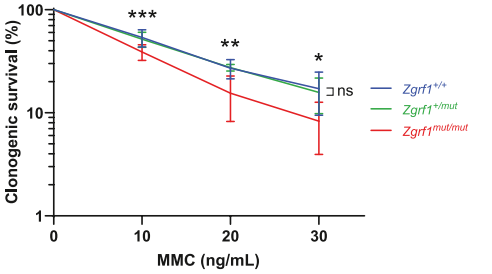

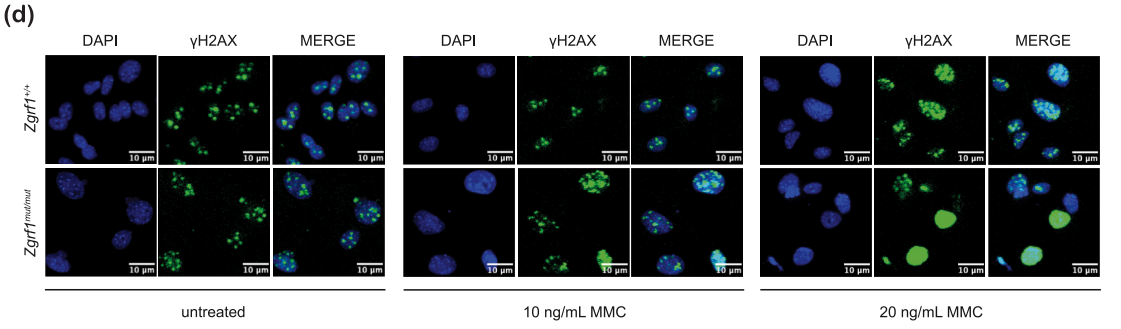

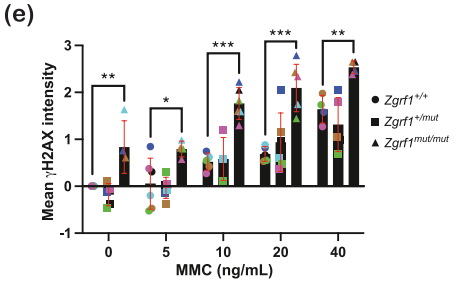

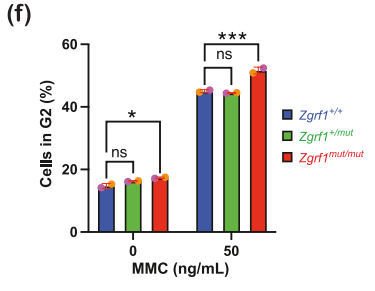

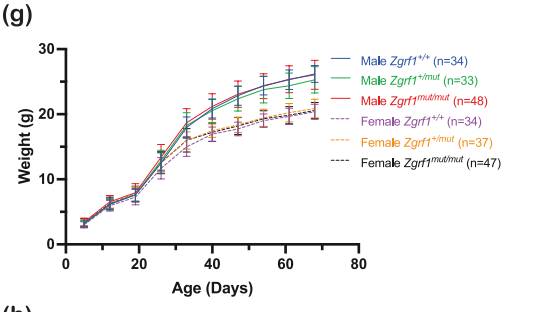

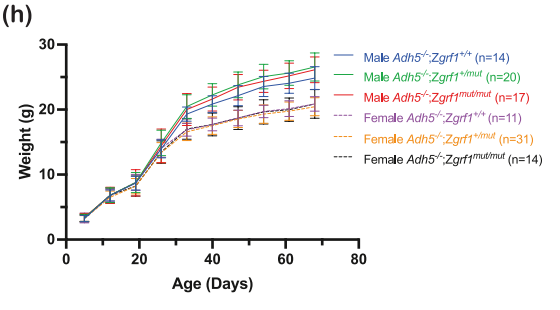

(caption on next page)

Fig. 1. Generation and characterisation of the *Zgrf1* mutant mouse. (a) Schematic diagram showing the targeted region of chromosome 3 where *Zgrf1* (Accession: NM_197997.2) is located. A frameshift mutation was induced through the introduction of a 5-base pair deletion in exon 4 using the CRISPR-Cas9 gene editing technique. This results in the premature termination of translation at the N-terminal DUF2439 domain. Amino acid numbers are shown above the schematic, with the conserved zinc finger (ZnF) and helicase domains indicated (not to scale). (b) Mendelian table depicting the distribution of the different genotypes in progenies born to heterozygous *Zgrf1* parents. (c) Clonogenic survival of *Zgrf1* MEFs treated with the indicated doses of MMC for 24 h. The assay was performed for three MEF lines of each genotype, derived from three different matings. The experiment was performed twice for each of the two first batches of cell lines and three times for the final batch (n = 7). Colony forming units were normalised to the untreated condition. The P values for the comparison of $Zgrf1^{+/+}$ and $Zgrf1^{mut/mut}$ are shown. (d–e) Quantification of γH2AX intensities in MEFs treated with the indicated doses of MMC. The data correspond to an average of >700 cells per condition (n = 4–6). The mean γH2AX intensity of untreated WT MEFs was set to zero. Colours of symbols in panel (e) indicate independent biological replicates. (f) Quantification of G2 phase MEFs under unperturbed conditions and in response to MMC treatment (n = 2). (g) Growth curve of *Zgrf1* mutant mice derived from their weekly weight recordings over a period of 10 weeks. (h) Growth curve of the *Adh5* KO mice. All graphs show the mean with SD, and statistical significance was assessed using 2-way ANOVA analysis. *P ≤ 0.05; **P ≤ 0.01; ***P ≤ 0.001; ns: not significant.

protein synthesis prematurely in the middle of the N-terminal domain of unknown function 2439 (DUF2439), eliminating 98 % of the coding capacity of ZGRF1 including the C-terminal helicase domain (Fig. 1a). To verify the absence of ZGRF1, mouse embryonic fibroblasts (MEFs) were cultured from homozygous $Zgrf1^{mut/mut}$ mice and analysed by western blotting (Fig. 2a), showing that expression of full-length Zgrf1 is abolished. The $Zgrf1^{mut/mut}$ mice were born at normal Mendelian ratios (Fig. 1b). At 8 weeks of age, they did not appear to exhibit any observable phenotypic abnormalities, and had similar overall brain, liver, thymus, spleen, testis, and femur tissue architecture as their wild-type (WT) counterparts (Fig. 2b and c). Given that ZGRF1 has been associated with brain disorders in human [21,22], we further determined the molecular layer interneuron density in the cerebellum as a general measure for neuronal proliferation, migration, and differentiation [28], but no significant difference was observed between WT and $Zgrf1^{mut/mut}$ (Fig. 2d).

Brannvoll et al. reported previously that the human ZGRF1 is involved in the repair of DSB intermediates that form downstream of the FA pathway [19]. To test if the mouse ZGRF1 helicase is also involved in DNA repair, $Zgrf1^{mut/mut}$ MEFs were subjected to MMC treatment. Results showed that $Zgrf1^{mut/mut}$ MEFs exhibit increased sensitivity to MMC across all examined concentrations, accompanied by increased γH2AX immunostaining compared to the WT MEFs under both untreated and treated conditions (Fig. 1c–e). Along with an increased accumulation in the G2/M phase under both untreated and MMC-treated conditions (Fig. 1f), these observations indicate that ZGRF1 also contributes to ICL repair in mice, and in the absence of ZGRF1, DSBs can accumulate, leading to G2-M checkpoint activation and cell cycle arrest [29].

One of the key players of the FA pathway is FANCD2, which forms the ID2 complex with FANCI [30]. Through monoubiquitylation of FANCD2, ID2 mediates the recruitment of downstream repair factors necessary for the subsequent steps of unhooking and repair [31,32]. Mice lacking FANCD2 display developmental defects both *in utero* and postnatally, appearing significantly smaller in size compared to the controls. Additionally, *Fancd2* KO mice exhibit perinatal mortality, microphthalmia, reduced germ cells in the testes and ovaries, and the onset of tumours across various epithelial cell types at a median age of 18 months [33]. Given that ZGRF1 colocalises with FANCD2 in human cells [19], we investigated whether the absence of ZGRF1 would result in any developmental delay in mice. The $Zgrf1^{mut/mut}$ mice were monitored from postnatal day 5 until they reached the age of 10 weeks, with their weight being recorded at weekly intervals (Fig. 1g). With similar average weights to the WT mice across all timepoints, there were no indications of developmental abnormalities in the $Zgrf1^{mut/mut}$ mice.

To further investigate the association of ZGRF1 with the FA pathway, the $Zgrf1^{mut}$ allele was introduced into *Adh5* KO mice through controlled mating to generate mice that are deficient for both ADH5 and ZGRF1. Cells that lack ADH5 fail to metabolise endogenous formaldehyde, leading to its accumulation that can cause DNA-protein crosslinks (DPCs) or ICLs [34–37]. In addition to ADH5, which provides the first line of defence against formaldehyde, the FA pathway acts as a secondary layer of protection against this compound [38,39]. In *Adh5* KO mice, formaldehyde accumulation was observed in the bone marrow, kidneys, and liver, predisposing them to hepatocellular carcinomas and adenomas as they age [39,40]. With the disruption of the FA pathway, these phenotypes became more prominent. $Adh5^{-/-}$;$Fancd2^{-/-}$ pups appeared approximately 32 % smaller in size compared to the WT littermate controls, exhibiting signs of blood pancytopenia and reduced bone marrow cellularity that culminated in complete hematopoietic failure within 3–7 weeks after birth [39].

Given its functional association with the FA pathway, we hypothesised that the lack of ZGRF1 could disrupt the protection against formaldehyde. If this hypothesis were to hold true, we would expect $Adh5^{-/-}$;$Zgrf1^{mut/mut}$ mice to display abnormalities similar to those observed in $Adh5^{-/-}$;$Fancd2^{-/-}$ mice during development. As *Adh5* and *Zgrf1* are linked on the same chromosome, a male $Adh5^{-/-}$;$Zgrf1^{+/mut}$ was bred with a female $Adh5^{-/-}$;$Zgrf1^{+/mut}$ to obtain the $Adh5^{-/-}$;$Zgrf1^{mut/mut}$ mice. The double mutants were born at normal Mendelian ratios without any abnormalities, and they displayed normal body weights and were able to survive beyond 30 weeks (Figs. 1h and 3a, b). These observations indicate that although ZGRF1 is involved in the FA pathway *in vitro*, its deficiency does not cause any phenotypic abnormalities in *Adh5*-deficient mice.

2.2. Impact of Zgrf1 mutant in cancer models

While elevated mutation rates can facilitate cell transformation and tumour progression, they can also compromise cell viability by surpassing cytotoxicity thresholds. Through controlled mating, the $Zgrf1^{mut}$ allele was introduced into the Eμ-*Myc* and *Trp53* cancer models to assess the role of ZGRF1 in tumorigenesis. The Eμ-*Myc* mouse harbours a transgene encoding the *Myc* proto-oncogene

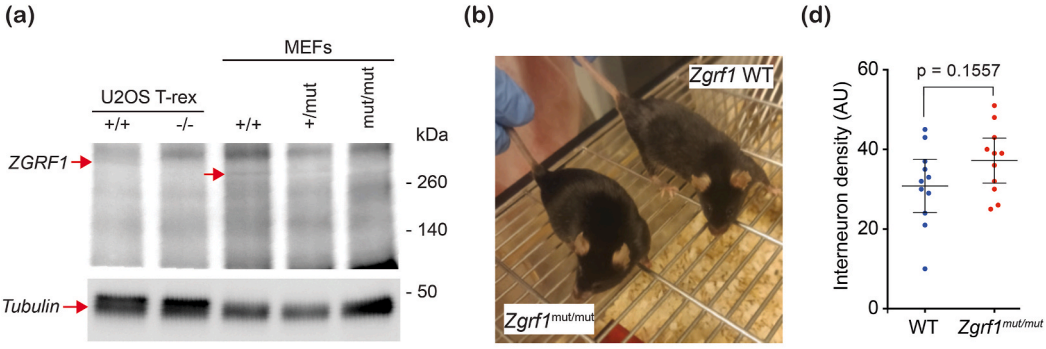

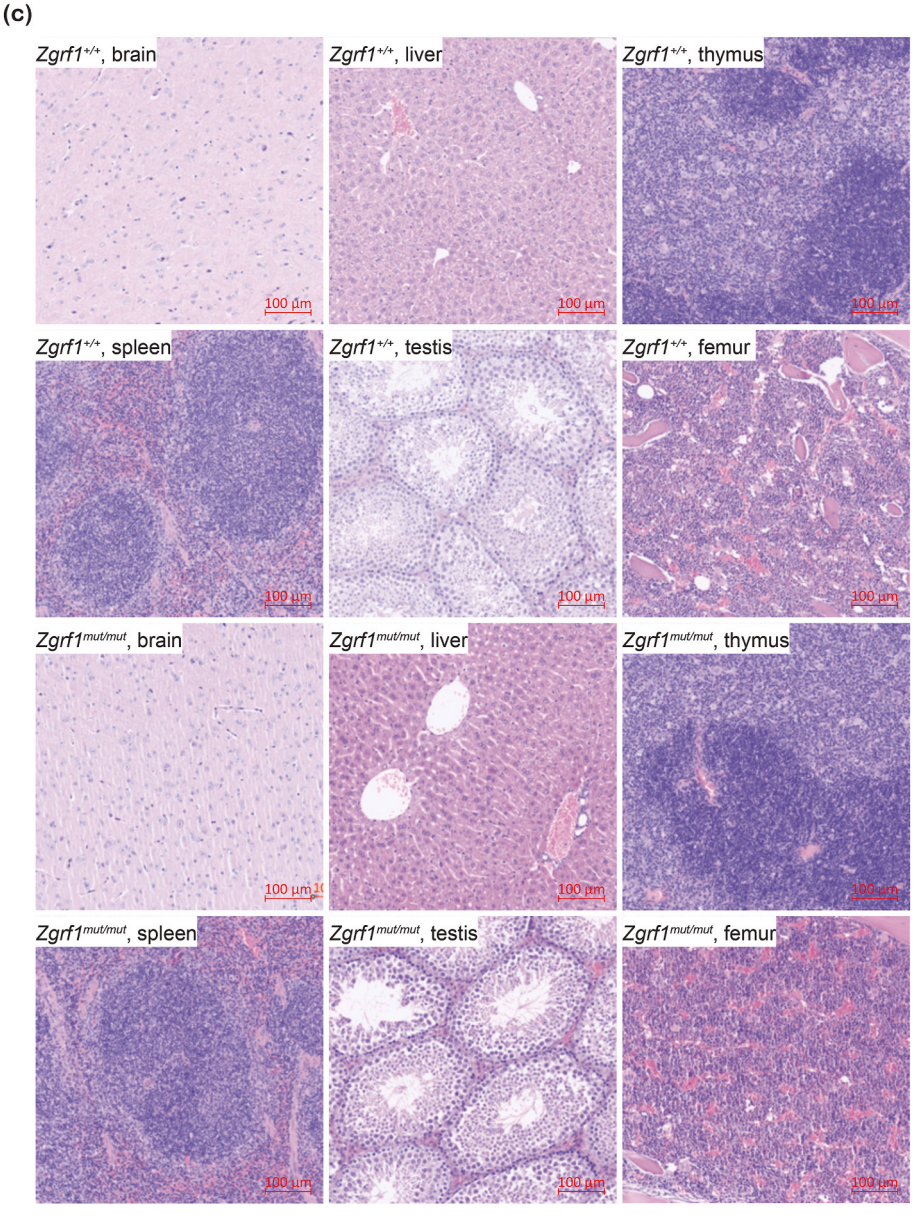

(caption on next page)

Fig. 2. Additional data from the characterisation of the *Zgrf1* mutant mouse. (a) Western blotting for the detection of *Zgrf1* in MEFs generated from the *Zgrf1*$^{mut/mut}$ mouse. The positive and negative controls used were the WT and *ZGRF1* KO U2OS T-rex cells, respectively (Human ZGRF1: 236.6 kDa; Mouse ZGRF1: 205.7 kDa). (b) Appearance of adult WT and *Zgrf1*$^{mut/mut}$ mice. (c) Representative H&E-stained sections of the brain, liver, thymus, spleen, testis, and femur histology prepared from 8-week-old WT and *Zgrf1*$^{mut/mut}$ mice. (d) Quantification of molecular layer interneuron density. Eleven random cerebellum regions of sagittal sections from WT and *Zgrf1*$^{mut/mut}$ were analysed. Error bars show SEM.

(a)

Cross: *Adh5*$^{-/-}$;*Zgrf1*$^{+/mut}$ x *Adh5*$^{-/-}$;*Zgrf1*$^{+/mut}$					
Genotype	**Observed**	**Value**	**Expected**	**Freq. observed (%)**	**Freq. expected (%)**
Adh5$^{-/-}$;*Zgrf1*$^{mut/mut}$	18	Low	20.75	21.69	25
Adh5$^{-/-}$;*Zgrf1*$^{+/mut}$	38	Low	41.5	45.78	50
Adh5$^{-/-}$;*Zgrf1*$^{+/+}$	27	High	20.75	32.53	25
Total	83		83	100	100
			Chi-square calculated value:	2.542	MENDELIAN
			Chi-square table:	5.991	
			Confidence level:	0.05	
			Calculated p-value:	0.281	
			Degrees of freedom:	2	

(b)

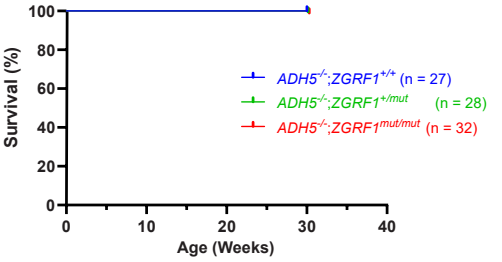

(c)

Cross: Eμ-*Myc*;*Zgrf1*$^{+/mut}$ x *Zgrf1*$^{+/mut}$					
Genotype	**Observed**	**Value**	**Expected**	**Freq. observed (%)**	**Freq. expected (%)**
Eμ-*Myc*;*Zgrf1*$^{mut/mut}$	39	Low	40.13	12.15	12.5
Zgrf1$^{mut/mut}$	38	Low	40.13	11.84	12.5
Eμ-*Myc*;*Zgrf1*$^{+/mut}$	63	Low	80.25	19.63	25.0
Zgrf1$^{+/mut}$	80	Low	80.25	24.92	25.0
Eμ-*Myc*;*Zgrf1*$^{+/+}$	50	High	40.13	15.58	12.5
Zgrf1$^{+/+}$	51	High	40.13	15.89	12.5
Total	321		321	100	100
			Chi-square calculated value:	9.23	MENDELIAN
			Chi-square table:	11.070	
			Confidence level:	0.05	
			Calculated p-value:	0.100	
			Degrees of freedom:	5	

(d)

Cross: *Trp53*$^{+/-}$;*Zgrf1*$^{+/mut}$ x *Trp53*$^{+/-}$;*Zgrf1*$^{+/mut}$ (Males)					
Genotype	**Observed**	**Value**	**Expected**	**Freq. observed (%)**	**Freq. expected (%)**
Trp53$^{+/-}$;*Zgrf1*$^{mut/mut}$	16	Low	17.56	5.69	6.25
Trp53$^{-/-}$;*Zgrf1*$^{+/mut}$	38	High	35.13	13.52	12.50
Trp53$^{-/-}$;*Zgrf1*$^{+/+}$	20	High	17.56	7.12	6.25
Trp53$^{+/-}$;*Zgrf1*$^{mut/mut}$	34	Low	35.13	12.10	12.50
Trp53$^{+/-}$;*Zgrf1*$^{+/mut}$	78	High	70.25	27.76	25.00
Trp53$^{+/-}$;*Zgrf1*$^{+/+}$	35	Low	35.13	12.46	12.50
Trp53$^{+/+}$;*Zgrf1*$^{mut/mut}$	12	Low	17.56	4.27	6.25
Trp53$^{+/+}$;*Zgrf1*$^{+/mut}$	29	Low	35.13	10.32	12.50
Trp53$^{+/+}$;*Zgrf1*$^{+/+}$	19	High	17.56	6.76	6.25
Total	281		281	100	100
			Chi-square calculated value:	4.55	MENDELIAN
			Chi-square table:	15.507	
			Confidence level:	0.05	
			Calculated p-value:	0.804	
			Degrees of freedom:	8	

(e)

Cross: *Trp53*$^{+/-}$;*Zgrf1*$^{+/mut}$ x *Trp53*$^{+/-}$;*Zgrf1*$^{+/mut}$ (Females)					
Genotype	**Observed**	**Value**	**Expected**	**Freq. observed (%)**	**Freq. expected (%)**
Trp53$^{-/-}$;*Zgrf1*$^{mut/mut}$	12	Low	12.94	5.80	6.25
Trp53$^{-/-}$;*Zgrf1*$^{+/mut}$	19	Low	25.88	9.18	12.50
Trp53$^{-/-}$;*Zgrf1*$^{+/+}$	4	Low	12.94	1.93	6.25
Trp53$^{+/-}$;*Zgrf1*$^{mut/mut}$	40	High	25.88	19.32	12.50
Trp53$^{+/-}$;*Zgrf1*$^{+/mut}$	62	High	51.75	29.95	25.00
Trp53$^{+/-}$;*Zgrf1*$^{+/+}$	25	Low	25.88	12.08	12.50
Trp53$^{+/+}$;*Zgrf1*$^{mut/mut}$	13	High	12.94	6.28	6.25
Trp53$^{+/+}$;*Zgrf1*$^{+/mut}$	22	Low	25.88	10.63	12.50
Trp53$^{+/+}$;*Zgrf1*$^{+/+}$	10	Low	12.94	4.83	6.25
Total	207		207	100	100
			Chi-square calculated value:	19.09	NON-MENDELIAN
			Chi-square table:	15.507	
			Confidence level:	0.05	
			Calculated p-value:	0.014	
			Degrees of freedom:	8	

Fig. 3. Supporting data from the Eμ-*Myc*, *Trp53* KO, *Trp53* het and *Adh5* KO breeding. (a, c, d & e) Mendelian tables depicting the distribution of the different genotypes in progenies born to parents as indicated. (b) Kaplan-Meier survival plot of the *Adh5* KO mice showing that the mutation of *Zgrf1* did not lead to premature mortality.

regulated by an immunoglobulin heavy chain enhancer. This enhancer facilitates the upregulation of *Myc* expression, driving B-cell hyperproliferation that leads to lymphomagenesis [25]. Eμ-*Myc*;*Zgrf1*$^{mut/mut}$ mice were born at normal Mendelian ratios (Fig. 3c) and did not exhibit any developmental issues, as evidenced by the recorded weights over a 10-week period (Fig. 4a). Despite a 10-week difference in median tumour-free survival age between the Eμ-*Myc*;*Zgrf1*$^{+/+}$ and Eμ-*Myc*; *Zgrf1*$^{mut/mut}$ mice, the Kaplan-Meier survival plot did not show significant differences regardless of whether ZGRF1 was mutated or not ($P = 0.8181$; Fig. 4b). This indicates that ZGRF1 did not present any survival advantage or disadvantage towards the development of Eμ-*Myc* driven tumours.

The p53 tumour suppressor mediates DNA repair and cellular senescence while also regulating the apoptotic pathway [41,42]. Commonly referred to as the Guardian of the Genome, the absence of p53 is frequently associated with cancers in both humans and mice [26,43,44]. As ZGRF1 is implicated in DNA repair and p53 is essential for the regulation of apoptosis, we hypothesised that in the absence of these two proteins, mutations can accumulate and propagate, accelerating tumorigenesis in the mouse. While *Trp53* KO

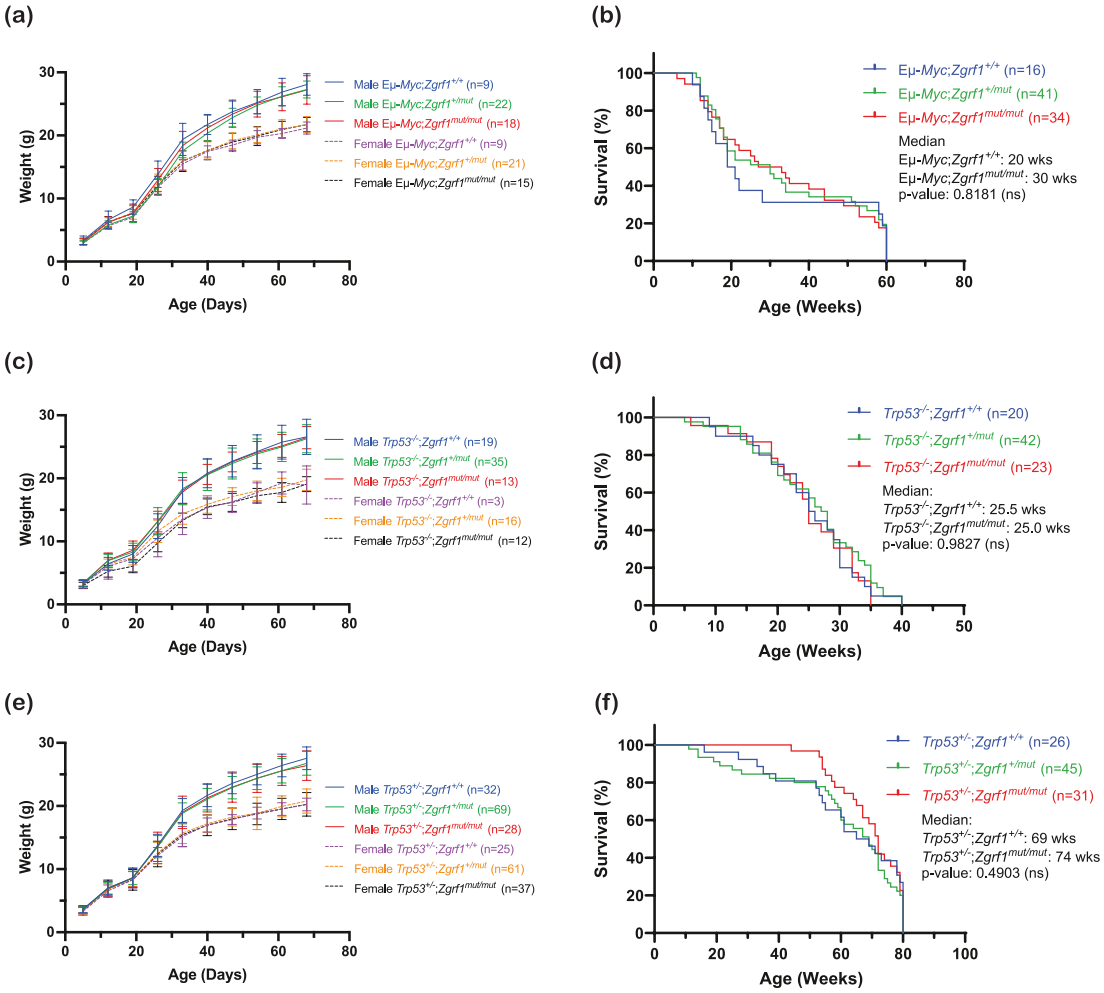

Fig. 4. Development curves of the various mouse strains examined and the survival curves of the Eμ-*Myc* and *Trp53* cancer models. (a, c & e) Growth curves of the Eμ-*Myc*, *Trp53* KO and *Trp53* het mice. (b, d and f) Kaplan-Meier survival plots of the Eμ-*Myc*, *Trp53* KO and *Trp53* het mice, with corresponding p-values derived from the log-rank (Mantel-Cox) test indicated on their respective graphs. The number of mice included in each cohort is shown in parentheses.

males of all *Zgrf1* genotypes were born at normal Mendelian ratios, *Trp53* KO females were significantly underrepresented regardless of their *Zgrf1* genotype (Fig. 3d and e). This phenomenon can be attributed to the role of p53 in promoting the proper establishment of X chromosome inactivation, enabling normal neural tube formation. In the absence of p53, neural tube defects manifest, leading to mortality during embryonic development or postnatally [45,46]. By monitoring their growth weekly, it was established that the $Trp53^{-/-}$;$Zgrf1^{mut/mut}$ males underwent normal development (Fig. 4c). The recorded median age of tumour-free survival was found to be similar for the $Trp53^{-/-}$;$Zgrf1^{+/+}$ and $Trp53^{-/-}$;$Zgrf1^{+/mut}$ mice. This suggests that ZGRF1 status does not impact the development of p53-associated cancers (Fig. 4d).

In conjunction with the *Trp53* KO mice, *Trp53* het mice were also assessed for early developmental abnormalities and their susceptibility to tumorigenesis during their lifespan. Similar to the $Trp53^{-/-}$;$Zgrf1^{mut/mut}$ mice, $Trp53^{+/-}$;$Zgrf1^{mut/mut}$ mice did not show any growth differences (Fig. 4e). Although *Trp53* het mice carry a functional copy of *Trp53*, chromosomal aberrations such as large-scale deletions, recombination or mitotic nondisjunction can cause loss of heterozygosity (LOH). This sporadically eliminates the function of p53 in some cells in these mice, predisposing them to cancer as they age [47]. From the Kaplan-Meier survival plot, the mutation of ZGRF1 in *Trp53* het mice marginally delays mortality, extending their median tumour-free survival age to 74 weeks compared to 69 weeks for $Trp53^{+/-}$;$Zgrf1^{+/+}$ mice ($P = 0.4903$; Fig. 4f). This suggests that the absence of ZGRF1 delays tumorigenesis or progression in *Trp53* het mice, promoting better survival.

2.3. ZGRF1 deficient mice are subfertile

An investigation of the fertility of *Zgrf1* mutant mice was prompted by observed chromosome segregation defects and failure to

dismantle Rad51 foci during meiosis I in the absence of the homolog of ZGRF1, Dbl2, in fission yeast [27]. To assess the impact of ZGRF1 deficiency on mouse fertility, *Zgrf1*$^{+/mut}$ and *Zgrf1*$^{mut/mut}$ breeding pairs were established. The time elapsed between the mating set up and appearance of the first litter, along with the size of the first four litters were recorded. A similar duration between the mating setup and appearance of the first litter for *Zgrf1* het and homozygous mutant breeding pairs was observed (Fig. 5a). However, the number of pups born to *Zgrf1*$^{mut/mut}$ parents was consistently lower across all four litters, with the difference being significant in the third litter (Fig. 5b). When comparing the average litter size, the number of pups from the *Zgrf1*$^{mut/mut}$ parents was significantly lower than the number of pups born to het parents. These findings prompted an examination of the reproductive organs to investigate if subfertility might be attributed to defects in gametogenesis.

The reduction in the number of germ cells in *Fancd2* KO mice was accompanied by a decrease in their testicular weight [33]. Similarly, when dissected and weighed, testes from the *Zgrf1*$^{mut/mut}$ mice were found to be physically smaller than the WTs, showing ~27 % reduction in the testis to body weight ratio (Fig. 5d and e). Histological examination of the testes did not reveal abnormalities in spermatogenesis, and every stage of spermatid was found to be present (Fig. 5f). Additional probing for cleaved caspase 3 (C3) did not reveal elevated levels of apoptosis (Fig. 5f). Since ZGRF1 promotes crossover formation via HR in mitotic cells [19], we hypothesised that it could also be involved in crossover formation during gametogenesis. To test this idea, meiotic chromosome spreads were prepared from *Zgrf1*$^{mut/mut}$ testes and stained for SYCP3 and MLH3, marking the synaptonemal complex and sites of meiotic crossovers, respectively (Fig. 5g) [48]. By quantifying the MLH3 foci, a reduction in the number of crossovers in the spermatocytes from the *Zgrf1*$^{mut/mut}$ mice was evident (Fig. 5h). This indicates that ZGRF1 could be involved in the promotion of crossover formation, allowing the homologous chromosomes to segregate properly during gametogenesis.

3. Discussion

Mice lacking *Fancd2* are predisposed to perinatal mortality and develop phenotypes such as developmental delays, microphthalmia and the reduction of germ cells in their reproductive organs [33]. Since ZGRF1 colocalises with FANCD2 to facilitate downstream DSB repair *in vitro*, we aimed to investigate the phenotype of *Zgrf1* mutant mice [19]. However, *Zgrf1*$^{mut/mut}$ mice developed normally without exhibiting any physical abnormalities (Fig. 1g), despite the *Zgrf1* mutant MEFs exhibiting increased sensitivity to ICL-inducing MMC (Fig. 1c). This could be attributed to the functional redundancy between ZGRF1 and other components within the FA pathway, allowing physiological ICL repair to proceed in its absence. This notion is consistent with the clonogenic survival assays previously reported by Brannvoll and colleagues to examine the epistasis of ZGRF1 with components of the FA pathway [19]. While ZGRF1 and FANCM were epistatic for MMC sensitivity, a negative genetic interaction was established between ZGRF1 and FANCJ. This suggests that in the absence of ZGRF1, the presence of FANCJ is allowing DSB repair downstream of the FA pathway to proceed [19]. Taken together, FANCJ may be ensuring the uninterrupted functionality of the FA pathway, thereby averting the manifestation of phenotypic abnormalities in the *Zgrf1*$^{mut/mut}$ mice.

We hypothesised that in the absence of ZGRF1, the ensuing genomic instability could affect the rate of tumorigenesis in Eμ-*Myc* mice through two possible means: it may either accelerate cellular transformation and tumorigenesis, or cause cytotoxic mutations to accumulate, compromising cell viability and slowing down the rate of tumour development. From the Kaplan-Meier survival plot (Fig. 4b), the median age of tumour-free survival observed for the Eμ-*Myc*;*Zgrf1*$^{+/+}$ and Eμ-*Myc*;*Zgrf1*$^{mut/mut}$ mice was 20 weeks and 30 weeks, respectively. However, the observed difference in median tumour-free survival age between these two groups did not reach significance ($P = 0.8181$), suggesting that ZGRF1 had no major impact on *Myc*-driven tumorigenesis. Perhaps, given the rapid development of tumours in the Eμ-*Myc* mice, ZGRF1 would need to play a greater role in the maintenance of genome stability to significantly influence the survival of these mice. However, the results of this survival study suggest otherwise, indicating that ZGRF1 plays a more subtle role in DNA repair in mice.

Likewise, we hypothesised that the lack of ZGRF1 in *Trp53* KO mice would accelerate tumorigenesis [19,33]. Based on the similar median age of tumour-free survival between these mice and their *Zgrf1* WT controls (Fig. 4d), this was not the case. One possible explanation could be that while the mutation of ZGRF1 can lead to genomic instability and cell transformation, it can also aggravate genomic instability in transformed cells, compromising their viability. This counteraction mitigates the influence of ZGRF1 mutation on tumorigenesis, resulting in a tumorigenesis rate similar to that of WT *Trp53* mice. By contrast, *Trp53* hets with mutation of *Zgrf1* exhibited marginally better survival than their corresponding *Zgrf1* WT controls ($P = 0.4903$; Fig. 4f). From the Kaplan-Meier survival plot, tumours appear to manifest later in *Trp53*$^{+/-}$;*Zgrf1*$^{mut/mut}$ mice, delaying their median age of tumour-free survival to 74 weeks. In contrast, *Trp53*$^{+/-}$;*Zgrf1*$^{+/+}$ and *Trp53*$^{+/-}$;*Zgrf1*$^{+/mut}$ mice exhibited a median survival age of 69 weeks, consistent with previous reports [49]. Correspondingly, it was reported that low expression of ZGRF1 in tumour tissue from patients is associated with increased overall survival [24]. Mice that are heterozygous for *Trp53* succumb to cancer due to a chromosomal event that disrupts the WT copy of *Trp53*, rendering them p53-null [47]. Also referred to as loss-of-heterozygosity (LOH), these events are HR-dependent, where genetic information is exchanged between non-sister chromatids [50]. Although mitotic recombination between homologs occurs at low frequencies, LOH events have been associated with approximately 40 % of the cases of hereditary retinoblastoma [51,52]. Since ZGRF1 is involved in HR repair, we consider the possibility that its mutation might reduce the frequency of LOH events, preserving the WT *Trp53* allele and thereby slowing down tumorigenesis in *Trp53* heterozygous mice. Histological examination of tumour tissues from these mice did not reveal a detectable level of p53 protein expression or its transcriptional product p21, indicating that LOH may have already occurred by the time tumours developed (Fig. 6).

Cells deficient for ADH5 and the FA pathway exhibited increased sensitivity to formaldehyde, and mice lacking ADH5 and FANCD2 experience early mortality [38,39,53,54]. As ZGRF1 is shown to colocalise with FANCD2 at MMC-induced foci, we anticipated that *Adh5*$^{-/-}$;*Zgrf1*$^{mut/mut}$ mice would develop phenotypic abnormalities. Contrary to our hypothesis, these mice were born at normal

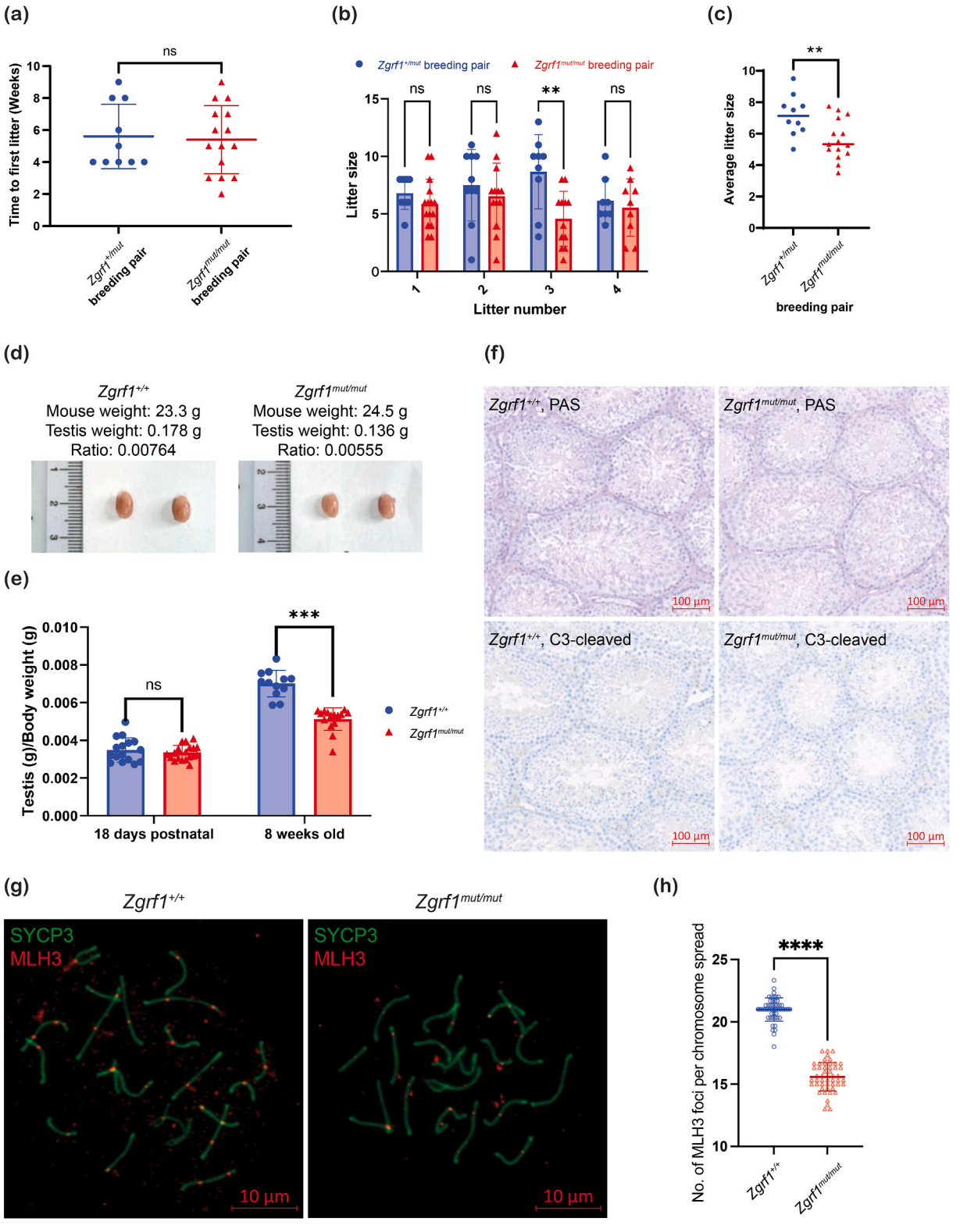

(caption on next page)

Fig. 5. Fertility analysis and the involvement of ZGRF1 in gametogenesis. 10 het and 15 KO breeding pairs were used for the fertility analysis in panels a, b and c. (a) Time elapsed between mating set up and the appearance of the first litter. (b) Litter size of the first four litters born to *Zgrf1*$^{+/mut}$ and *Zgrf1*$^{mut/mut}$ parents. (c) Average litter size from all *Zgrf1*$^{+/mut}$ and *Zgrf1*$^{mut/mut}$ breeding pairs. (d) Morphology of WT and *Zgrf1*$^{mut/mut}$ testes dissected from 8-week-old males. (e) Ratio between the testes and body weight of WT and *Zgrf1*$^{mut/mut}$ mice at 18 days postnatal (WT: n = 16, KO: n = 19) and 8 weeks (WT: n = 12, *Zgrf1*$^{mut/mut}$: n = 15). (f) Histology of WT and *Zgrf1*$^{mut/mut}$ testes stained with the PAS reagent and C3-cleaved caspase antibody. (g) Representative pachytene spermatocyte immunostained for SYCP3 (in green), a component of the synaptonemal complex, and MLH3 foci (in red) for detecting crossovers. (h) Quantification of MLH3 foci per chromosome spread showing a reduction in the number of crossovers events in *Zgrf1*$^{mut/mut}$ spermatocytes (3 animals, 50 spreads each) compared to WT (3 animals, 50 spreads each). All graphs show the mean with SD. Statistical significance was assessed using the unpaired *t*-test in (a), (c) and (h), and 2-way ANOVA analysis in (b) and (e). **P ≤ 0.01; ***P ≤ 0.001; ****P ≤ 0.0001; ns: not significant.

Mendelian ratios and did not display any adverse phenotypes. Consistently, clonogenic survival assays also revealed that human HCT116 cells lacking *ZGRF1* did not show sensitivity to formaldehyde (Fig. 7). However, while formaldehyde is shown to produce ICLs *in vitro*, there are no reports of formaldehyde-induced ICLs detected *in vivo* [35,36]. Moreover, although the FA pathway has been reported to be implicated in the repair of formaldehyde-induced DNA adducts, it has not been demonstrated to be associated with ICL repair in this context [38,39]. To our knowledge, the chemical nature of formaldehyde-induced DNA adducts that require the FA pathway for repair has not been elucidated. Therefore, a plausible explanation for the observed lack of impact on mouse mortality could be ZGRF1's non-association with this yet-to-be-identified repair pathway or redundancy of ZGRF1 with FANCJ in terms of repair of formaldehyde-induced lesions [19].

Through the fertility study, we established that the number of pups born to *Zgrf1*$^{mut/mut}$ parents was reduced, indicating that ZGRF1

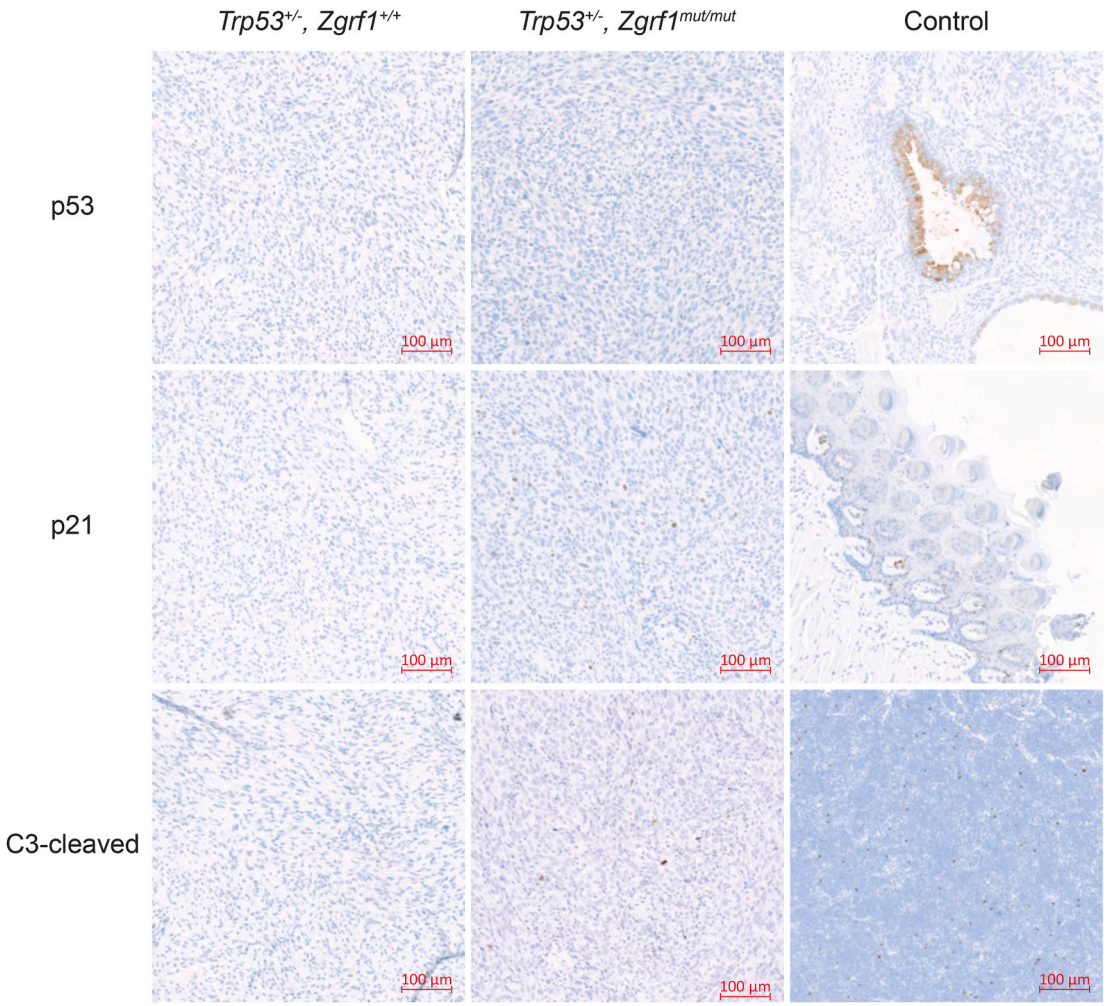

Fig. 6. Histology of tumours from *Trp53* het mice. Representative sections of tumours stained with antibodies for p53, p21 and C3-cleaved caspase to detect the presence of p53, its transcriptional regulatory function that induces p21 expression and its apoptotic function via the activation of caspases.

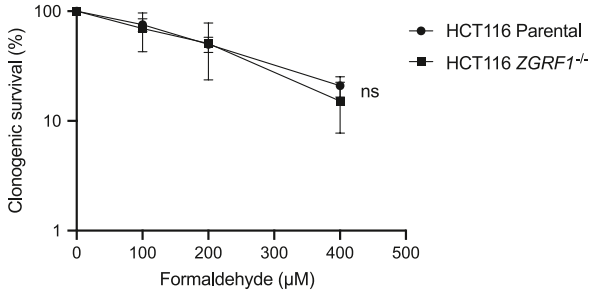

Fig. 7. Sensitivity of human cells to formaldehyde. Clonogenic survival assay of HCT116 parental and ZGRF1$^{-/-}$ cells in response to the indicated doses of formaldehyde for 1 h. $N \geq 3$ for each cell line. Graphs show the mean with SD. Statistical significance was calculated using multiple *t*-test. ns: not significant.

is associated with the reproductive capabilities of mice. Histology performed on the testes did not reveal any obvious defects in spermatogenesis, although the frequency of crossovers during spermatogenesis was reduced. Despite the significant reduction in crossover frequency, the histological examination did not reveal obvious abnormalities during the process of spermatogenesis. The formation of crossovers during meiosis is an obligatory event that ensures the proper segregation of homologous chromosomes during the first meiotic division [55]. Failure to establish crossovers can result in chromosomal nondisjunction and the formation of aneuploid gametes. As aneuploidy is associated with infertility [56], the decrease in litter size observed from *Zgrf1*$^{mut/mut}$ breeding pairs could be attributed to embryonic lethality resulting from the fertilisation between aneuploid gametes similar to that observed for hypomorphic variants of human MLH1/MLH3, which exhibit reduced meiotic recombination [57]. While the meiotic phenotype of *Zgrf1* mutant mice could be explained by a direct effect on RAD51 function, transcriptomics analysis of *dbl2*Δ cells in *S. pombe* suggests that ZGRF1 could also have a function in regulation of meiotic gene expression [58].

4. Materials and methods

4.1. Declarations

All animal experiments were performed in compliance with the guidelines laid out by the Federation of European Laboratory Animal Science Associations (FELASA) and the Danish Animal Experiments Inspectorate. Experimental mice were housed in the animal facilities of the Department of Experimental Medicine at the University of Copenhagen under standard conditions, where they were provided with a rodent chow diet and water ad libitum. These mice were closely monitored and were euthanised at the earliest symptom of discomfort, or when tumour growth exceeds the maximum size allowed (www.dyreforsoegstilsynet.dk) (license numbers 2021-15-0201-00803; 2020-15-0201-00723; 2020-15-0201-00679). All euthanasia procedures were performed by cervical dislocation.

4.2. Mouse model generation

The *Zgrf1* mutant mouse employed in this study was created in collaboration with the Core Facility for Transgenic Mice at the University of Copenhagen. Using the CRISPR/Cas9 technology outlined in Ref. [59], a single guide RNA (GCGATTTTATATGATGA-CAA-AGG) was designed to induce indels into *Zgrf1* (MGI:1918893). This resulted in a 5-base pair deletion in exon 4, which we name *Zgrf1*^{em1Ucph}. This frameshift mutation is predicted to cause protein synthesis to terminate prematurely. Truncated in the middle of the DUF2439 domain, the putative peptide expressed from the mutated locus represents less than 2 % of the ZGRF1 wild-type protein. In brief, the guide RNA (20 ng/μL) and Cas9 mRNA (50 ng/μL) were co-injected into the pronuclei and the cytoplasm of C57BL/6N inbred zygotes. Subsequently, these embryos were transferred into a pseudo-pregnant female mouse for development, leading to the production of progenies. Sequencing of the *Zgrf1* exon 4 was performed to confirm the deletion, after which a founder mouse was selected to establish the *Zgrf1*$^{mut/mut}$ strain. Through crossbreeding of the *Zgrf1* mutant strain with the Eμ-*Myc* (MGI: 2447604), *Trp53* KO (MGI: 1857590), and *Adh5* KO (MGI: 5049924) strains, the Eμ-*Myc*;*Zgrf1*$^{mut/mut}$, *Trp53*$^{-/-}$;*Zgrf1*$^{mut/mut}$, *Trp53*$^{+/-}$;*Zgrf1*$^{mut/mut}$, and *Adh5*$^{-/-}$;*Zgrf1*$^{mut/mut}$ mice used in this study were generated. Genotyping of mice was performed by Transnetyx using real-time PCR.

4.3. Cell culture

MEFs were generated from 13.5 days post coitum (dpc) mouse embryos in accordance with standard procedures (http://jacks-lab.mit.edu/protocols/making_mefs). The heads of the embryos were used for genotyping (Transnetyx). MEFs were cultured in Dulbecco's Modified Eagle Medium (DMEM; Gibco) supplemented with 15 % heat-inactivated foetal bovine serum (FBS; ThermoFisher Scientific) and 1 % penicillin-streptomycin (ThermoFisher Scientific). Prior to their use in experiments, western blotting was performed in accordance with the procedures described in Ref. [19] to verify the absence of ZGRF1. In brief, cells were grown in a 150 cm Petri dish. Once they reached 80 % confluency, cells were washed once with PBS and collected using cell scrapers. Cells were centrifuged at

250×*g* for 5 min at 4 °C, supernatant was removed, and cells were re-suspended in 800 μL ice-cold PBS. This was followed by centrifugation at 2500×*g* for 30 s at 4 °C and re-suspension in 1.8 mL NP-40 buffer (150 mM NaCl, 1 % NP-40, 50 mM Tris-HCl pH 8.0, 1 mM PMSF, complete protease inhibitor cocktail (Roche, cat. no. 25735720)). Samples were lysed by syringing through a 23G needle 10 times on ice and centrifuged at 13000×*g* for 20 min at 4 °C. The supernatant was used for pulldown of ZGRF1 using Dynabeads Protein G (Life Technologies, cat. no. 10004D) according to the manufacturer's instructions. To each sample of beads, 2.42 μg anti-ZGRF1 rabbit antibody (BioGenes GmbH, custom-made rabbit polyclonal anti-ZGRF1, lot no. 28429; available upon request) and 1 μg rat anti-tubulin antibody (Abcam, cat. no ab6160) were bound. PBS with 0.1 % Tween-20 was used as washing buffer. Samples were eluted in 1X SDS sample buffer (2X SDS sample buffer (125 mM Tris-HCl pH 6.8, 5 % SDS, 0.004 % Bromophenol Blue, 10 % beta-mercaptoethanol, 20 % glycerol) diluted 1:2 in RIPA buffer (150 mM NaCl, 1 % NP-40, 0.5 % sodium deoxycholate, 0.1 % SDS, 50 mM Tris-HCl pH 8.0, 1 mM PMSF, complete protease inhibitor cocktail)) at 70 °C with shaking at 1000 RPM for 10 min. Eluted samples were boiled, run on an 4–20 % gradient SDS-PAGE gel (Bio-Rad cat.no. 4561094) until the 40 kDa marker ran out of the gel, and transferred to a 0.45 μm ethanol activated PVDF membrane 0.45 μm (Thermo Fisher, cat. no. 88585) at 40 mA for 18 h at 4 °C in an ice bucket. The membrane was cut at 60 kDa to separate tubulin from ZGRF1 and blocked with anti-ZGRF1 (1:1000 dilution in 5 % BSA (Merck, cat.no. A4503)) and with anti-tubulin (1:20.000 dilution in 5 % skim milk (Millipore, cat. no. 70166)) in TBST for 1 h at room temperature with gentle shaking followed by 3 washes with TBST for 10 min. Each membrane was incubated with their respective primary antibodies at 4 °C overnight (1:1000 rabbit anti-ZGRF1 (BioGenes GmbH, lot no. 28429) in 5 % BSA in TBST or 1:20.000 rat anti-tubulin (Abcam, cat. no ab6160) in 5 % milk in TBST). Membranes were washed 3 times with TBST for 10 min and incubated with respective secondary antibodies (1:1000 swine anti-rabbit (Dako, cat no. P0217) for ZGRF1 and 1:2000 rabbit anti-rat (Dako, cat. no. P0450) for tubulin) in 5 % skim milk in TBST for 1 h followed by another 3 washes for 10 min in TBST. For visualisation of secondary antibodies, ECL mixture (GE Healthcare, cat. no. RPN2232) was prepared and added to the membrane followed by imaging of chemiluminescence (ImageQuant LAS 4000). For the colony survival assay, three MEF lines of each genotype, derived from three different matings, were used. The experiment was performed twice for each of the two first batches of cell lines and three times for the final batch (n = 7). MEFs used in cell cycle profiling and high-content imaging were derived from the same mating.

4.4. Colony survival assay

Early-passage MEFs (*Zgrf1*$^{+/+}$, *Zgrf1*$^{+/mut}$ and *Zgrf1*$^{mut/mut}$) were plated onto a 6-well plate in duplicates at a density of 20,000 cells per well. MMC (Sigma, cat. no. M7949) was added at the indicated concentrations, and cells were incubated for 24 h, before they were rinsed and replaced with fresh medium. The cells were then allowed to grow for 10 days, with media replacement every three days. After 10 days of growth, the cells were fixed in methanol:acetic acid (3:1) and stained with crystal violet in methanol. The surviving fraction at each drug concentration was calculated based on the colony numbers and normalised to the corresponding untreated samples.

4.5. Cell cycle profiling

Prior to MMC treatment, 10^6 cells were seeded in 10 cm dishes and incubated O/N for adherence. After incubation, cells were treated with 50 ng/mL of MMC (Sigma, cat. no. M7949) for 72 h at 37 °C. Cells were harvested the next day by trypsinisation, spun down at 300×*g* for 5 min, resuspended in 1 mL of PBS and filtered through a 50 mm filter (BD Biosciences, cat no. 340629) directly into ice-cold 70 % ethanol for fixation. Once fixed, cells were stained with propidium iodide as described in Ref. [60], and the cell cycle distribution was analysed using the BD FACSJazz Cell Sorter (BD Biosciences, cat. no. 655490).

4.6. High content imaging

MEFs were seeded at a concentration of 2×10^4 cells/well onto μCLEAR 96-well plates (Greiner Bio-One, 655090) and incubated for 48 h before MMC treatment. In the next step, cells were treated with the indicated concentrations of MMC (Sigma, cat. no. M7949) for 4 h at 37 °C, before being fixed with 4 % formaldehyde for 10 min at room temperature (RT). The fixed cells were washed twice with PBS, before being permeabilised with 0.5 % Triton X-100 in PBS. Cells were then blocked (2.5 % BSA in PBST) for an hour at RT, after which they were incubated overnight at 4 °C with the primary γH2AX antibody (Merck Millipore 05–636). An anti-mouse secondary antibody conjugated to Alexa Fluor 488 (Sigma-Aldrich A-11001) was used for detection, and the nuclei were stained for 10 min at RT with 2 μg/mL DAPI. High-content microscopy was performed with the automated Olympus IX83 ScanR microscope (20x objective), and signal densities from the images were analysed using the ScanR software (Olympus).

4.7. Immunohistochemistry

Histological analyses were performed in collaboration with the Histopathology Core Unit at the Spanish National Cancer Research Centre (CNIO, Madrid, Spain). Mouse tissues and tumours were fixed in 4 % neutral buffered formalin (Sigma-Aldrich), paraffin-embedded, and processed according to standard procedures. Sections of 3 μm thickness were stained with Haematoxylin & Eosin (H&E). In addition to H&E staining, mouse testes were stained with Periodic acid-Schiff (PAS) reagent to differentiate spermatogonia types and stages of spermatogenesis. Depending on the type of primary antibody, one of the three automated platforms available at CNIO was utilised for immunostaining (Dako-Autostainer Plus, Leica-Bond MAX, or Roche-BenchMark Ultra). The primary antibodies used in this study were Cleaved Caspase-3 (Asp175) (Cell Signalling Technology, #9661), p21 (CNIO, 291H/B5), and p53 (CNIO,

POE316 A/E9), and the nuclei were counterstained using Carazzi's haematoxylin. Slides were digitalised using the ZEISS Axioscan.Z1 microscope and visualised using the Zen Lite software (ZEISS).

4.8. Meiotic chromosomal analysis

To analyse crossover events occurring during prophase I, meiotic chromosome spreads were prepared from mouse spermatocytes as described [61]. In brief, testes of WT and *Zgrf1*$^{mut/mut}$ males were harvested at postnatal day 18. The tunica was removed, and the seminiferous tubules were incubated in Hypotonic Extraction Buffer for 30 min (30 mM Tris-Cl, pH 8.2, 50 mM sucrose, 17 mM trisodium citrate dihydrate, 5 mM EDTA, 0.5 mM dithiothreitol and 0.1 mM phenylmethylsulfonyl fluoride in Milli-Q water, pH adjusted to 8.2–8.4). The seminiferous tubules were then transferred onto a Teflon-printed 3-ring slide containing 20 μL of 100 mM sucrose and minced to release the spermatocytes. These cells were then mixed with a freshly made fixative solution (1 % paraformaldehyde and 0.15 % Triton X-100 in PBS, pH 9.2), spread across a glass slide and incubated in a humidified chamber for fixation. After 2–2.5 h, the humidified chamber was cracked open to allow slides to dry completely. These slides were then subjected to a final wash in 0.4 % Photo-flo (Kodak, 1464510) and air-dried to prepare them for staining.

Immunofluorescence staining was performed using the procedure modified from Ref. [62]. The primary antibodies used were Anti-SCP-3 Antibody (D-1) raised in mouse (Santa Cruz; sc-74569, 1:1000) and anti-MLH3 antibody raised in rabbit (gifted by Paula E. Cohen, 1:500). Slides were blocked in 10X antibody dilution buffer (ADB) containing 3 g Bovine Serum Albumin (Sigma-Aldrich, A4503), 10 mL Normal Goat Serum (Gibco™, PCN5000) and 250 μL 20 % Triton-X in 90 mL of PBS. Slides were incubated with primary antibodies diluted in 1X ADB overnight in a humidified chamber, after which they were washed and incubated with the secondary antibodies for an hour. Secondary antibodies used were Goat anti-Mouse IgG Alexa Fluor™ Plus 488 (ThermoFisher, A32723, 1:1000) and Goat anti-Rabbit Alexa Fluor™ 594 (ThermoFisher, A-11012, 1:1000). Final washes were performed, and the slides were dried. To prepare the slide for imaging, the DAPI mounting media (4 % n-propyl gallate, 80 % glycerol and 1.5 mg/mL DAPI) was added and a coverslip was applied. Cells were visualised using the ZEISS Axio Imager Z2 and the MLH3 foci from pachynema cells were manually counted.

4.9. Clonogenic survival after formaldehyde treatment

The human HCT116 parental and *ZGRF1*$^{-/-}$ cell lines [19] were plated in duplicate in 40 % conditioned McCoy's 5A (Modified) medium (Life Technologies, cat. no. 26600023), containing 10 % heat-inactivated FBS (Gibco by Life Technologies, cat. no. 10500-064), and 10,000 units/mL of penicillin and 10,000 μg/mL of streptomycin (Gibco by Life Technologies, cat. no. 15140-122) and were then allowed to adhere overnight followed by treatment with the indicated doses of formaldehyde (Sigma, cat. no. 252549). One hour after drug addition, cells were washed with fresh media and incubated for 8 days in fresh growth media. Human cell lines used in this study are listed in Table 1.

4.10. Statistical analysis

Statistical analysis for the distribution of genotypes from the mouse crosses were determined using the Pearson's χ^2 test as described [65]. All other statistical analyses were performed using GraphPad Prism version 10.1.2 for Windows, GraphPad Software (www.graphpad.com). The significance was determined using either an unpaired *t*-test or two-way ANOVA with multiple comparisons. For all Kaplan-Meier survival curve analyses, the log-rank (Mantel-Cox) test was used for the determination of the p-values. *In vitro* experiments were performed with at least three biological replicates, except cell cycle profiling which was done in duplicates.

CRediT authorship contribution statement

Ernest Wee Kiat Lim: Writing – original draft, Visualization, Methodology, Investigation, Formal analysis. **Smaragda Kompocholi:** Writing – review & editing, Methodology, Investigation. **André Brannvoll:** Writing – review & editing, Methodology, Investigation. **K. Stine V. Bagge:** Writing – review & editing, Methodology, Investigation. **Jennifer R. Gruhn:** Writing – review & editing, Supervision, Funding acquisition. **Javier Martin-Gonzalez:** Writing – review & editing, Methodology. **Eliene Albers:** Writing – review & editing, Methodology, Investigation. **Ian D. Hickson:** Writing – review & editing, Supervision, Funding acquisition. **Andrés López-Contreras:** Writing – review & editing, Supervision, Formal analysis, Conceptualization. **Michael Lisby:** Writing – review & editing, Supervision, Project administration, Funding acquisition, Formal analysis, Data curation, Conceptualization.

Ethical approval

This study was reviewed and approved by the Danish Animal Experiments Inspectorate (Dyreforsøgstilsynet; https://dyreforsoegstilsynet.dk) with the approval license numbers 2021-15-0201-00803; 2020-15-0201-00723; 2020-15-0201-00679 dated 18-03-2021, 14-12-2020, and 16-11-2020, respectively.

Data availability statement

Data will be made available on request.

Table 1
Cell lines used in this study.

Name	Genotype	Parent	Reference
HCT116			[63]
ZGRF1 KO col. 25	ZGRF1$^{+1/-8}$	HCT116	[19]
U2OS	Flp-In T-REx		[64]
ZGRF1 KO col. 36	ZGRF1$^{+1/-7}$ Flp-In T-REx	U2OS	[19]

Declaration of competing interest

The authors declare the following financial interests/personal relationships which may be considered as potential competing interests: Michael Lisby reports financial support was provided by Novo Nordisk Foundation. Jennifer R. Gruhn reports financial support was provided by Novo Nordisk Foundation. Ian D. Hickson reports financial support was provided by Danish National Research Foundation. If there are other authors, they declare that they have no known competing financial interests or personal relationships that could have appeared to influence the work reported in this paper.

Acknowledgements

This study was supported by the Novo Nordisk Foundation (NNF19OC0055203 and NNF22OC0074308) to ML and JRG, respectively, and the Danish National Research Foundation (DNRF115) to ML, AL-C and IDH. We thank Ketan J. Patel for providing us with the cryopreserved *Adh5* KO sperm straws and Paula E. Cohen for providing us with the rabbit anti-MLH3 antibody. We would also like to thank Patricia González from the Histopathology Core Unit at CNIO, and the caretakers from the Mouse Genetic Unit for the technical assistance. Lastly, we thank Eva R. Hoffmann for advice on meiotic spreads.

References

[1] P.A. Jeggo, L.H. Pearl, A.M. Carr, DNA repair, genome stability and cancer: a historical perspective, Nat. Rev. Cancer 16 (2016) 35–42, https://doi.org/10.1038/nrc.2015.4.
[2] T. Lindahl, D.E. Barnes, Repair of endogenous DNA damage, Cold Spring Harbor Symp. Quant. Biol. 65 (2000) 127–133, https://doi.org/10.1101/sqb.2000.65.127.
[3] D. Hanahan, Hallmarks of cancer: new dimensions, Cancer Discov. 12 (2022) 31–46, https://doi.org/10.1158/2159-8290.CD-21-1059.
[4] C.M. Bielski, B.S. Taylor, Homing in on genomic instability as a therapeutic target in cancer, Nat. Commun. 12 (2021) 3663, https://doi.org/10.1038/s41467-021-23965-5.
[5] M.M. Vilenchik, A.G. Knudson, Endogenous DNA double-strand breaks: production, fidelity of repair, and induction of cancer, Proc. Natl. Acad. Sci. U. S. A. 100 (2003) 12871–12876, https://doi.org/10.1073/pnas.2135498100.
[6] W.J. Cannan, D.S. Pederson, Mechanisms and consequences of double-strand DNA break formation in chromatin, J. Cell. Physiol. 231 (2016) 3–14, https://doi.org/10.1002/jcp.25048.
[7] J.A. Kaye, J.A. Melo, S.K. Cheung, M.B. Vaze, J.E. Haber, D.P. Toczyski, DNA breaks promote genomic instability by impeding proper chromosome segregation, Curr. Biol. 14 (2004) 2096–2106, https://doi.org/10.1016/j.cub.2004.10.051.
[8] N. Chatterjee, G.C. Walker, Mechanisms of DNA damage, repair, and mutagenesis, Environ. Mol. Mutagen. 58 (2017) 235–263, https://doi.org/10.1002/em.22087.
[9] A. Kuzminov, Single-strand interruptions in replicating chromosomes cause double-strand breaks, Proc. Natl. Acad. Sci. U. S. A. 98 (2001) 8241–8246, https://doi.org/10.1073/pnas.131009198.
[10] J. Niraj, A. Farkkila, A.D. D'Andrea, The Fanconi anemia pathway in cancer, Annu. Rev. Cell Biol. 3 (2019) 457–478, https://doi.org/10.1146/annurev-cancerbio-030617-050422.
[11] A.T. Wang, T. Kim, J.E. Wagner, B.A. Conti, F.P. Lach, A.L. Huang, H. Molina, E.M. Sanborn, H. Zierhut, B.K. Cornes, et al., A dominant mutation in human RAD51 reveals its function in DNA interstrand crosslink repair independent of homologous recombination, Mol. Cell 59 (2015) 478–490, https://doi.org/10.1016/j.molcel.2015.07.009.
[12] D.T. Long, V. Joukov, M. Budzowska, J.C. Walter, BRCA1 promotes unloading of the CMG helicase from a stalled DNA replication fork, Mol. Cell 56 (2014) 174–185, https://doi.org/10.1016/j.molcel.2014.08.012.
[13] F. Zhang, Q. Fan, K. Ren, P.R. Andreassen, PALB2 functionally connects the breast cancer susceptibility proteins BRCA1 and BRCA2, Mol. Cancer Res. 7 (2009) 1110–1118, https://doi.org/10.1158/1541-7786.MCR-09-0123.
[14] S. Sigurdsson, S. Van Komen, W. Bussen, D. Schild, J.S. Albala, P. Sung, Mediator function of the human Rad51B-Rad51C complex in Rad51/RPA-catalyzed DNA strand exchange, Genes Dev. 15 (2001) 3308–3318, https://doi.org/10.1101/gad.935501.
[15] N. Ameziane, P. May, A. Haitjema, H.J. van de Vrugt, S.E. van Rossum-Fikkert, D. Ristic, G.J. Williams, J. Balk, D. Rockx, H. Li, et al., A novel Fanconi anaemia subtype associated with a dominant-negative mutation in RAD51, Nat. Commun. 6 (2015) 8829, https://doi.org/10.1038/ncomms9829.
[16] A.R. Venkitaraman, Linking the cellular functions of BRCA genes to cancer pathogenesis and treatment, Annu. Rev. Pathol. 4 (2009) 461–487, https://doi.org/10.1146/annurev.pathol.3.121806.151422.
[17] J. Michl, J. Zimmer, M. Tarsounas, Interplay between Fanconi anemia and homologous recombination pathways in genome integrity, EMBO J. 35 (2016) 909–923, https://doi.org/10.15252/embj.201693860.
[18] R.M. Brosh Jr., DNA helicases involved in DNA repair and their roles in cancer, Nat. Rev. Cancer 13 (2013) 542–558, https://doi.org/10.1038/nrc3560.
[19] A. Brannvoll, X. Xue, Y. Kwon, S. Kompocholi, A.K.W. Simonsen, K.S. Viswalingam, L. Gonzalez, I.D. Hickson, V.H. Oestergaard, H.W. Mankouri, et al., The ZGRF1 helicase promotes recombinational repair of replication-blocking DNA damage in human cells, Cell Rep. 32 (2020) 107849, https://doi.org/10.1016/j.celrep.2020.107849.
[20] C. Gao, N. Wang, X. Guo, J.T. Ziegler, K.D. Taylor, A.H. Xiang, Y. Hai, S.J. Kridel, J.L. Nadler, F. Kandeel, et al., A comprehensive analysis of common and rare variants to identify adiposity loci in hispanic Americans: the IRAS family study (IRASFS), PLoS One 10 (2015) e0134649, https://doi.org/10.1371/journal.pone.0134649.
[21] B. Peter, E.M. Wijsman, A.Q. Nato, Jr, M.M. G. Matsushita, K.L. Chapman, I.B. Stanaway, J. Wolff, K. Oda, V.B. Gabo, W.H. Raskind, University of Washington Center for Mendelian, Genetic candidate variants in two multigenerational families with childhood apraxia of speech, PLoS One 11 (2016) e0153864, https://doi.org/10.1371/journal.pone.0153864.

[22] S.R. Choudhury, P. Satishchandra, S. Sinha, A. Anand, ZGRF1 variants implicated in a sensory reflex epilepsy, bioRxiv (2019) 1–25, https://doi.org/10.1101/728188.

[23] W. Ge, M. Jiang, F. Zhang, Y. Ma, H. Wang, Y. Xu, ZGRF1 is associated with poor prognosis in triple-negative breast cancer and promotes cancer stemness based on bioinformatics, OncoTargets Ther. 13 (2020) 2843–2854, https://doi.org/10.2147/OTT.S234250.

[24] S. Yan, M. Song, J. Ping, S.T. Lai, X.Y. Cao, C.J. Bai, D.F. Xie, H. Guan, S.S. Gao, P.K. Zhou, ZGRF1 promotes end resection of DNA homologous recombination via forming complex with BRCA1/EXO1, Cell Death Dis. 7 (2021) 260, https://doi.org/10.1038/s41420-021-00633-7.

[25] J.M. Adams, A.W. Harris, C.A. Pinkert, L.M. Corcoran, W.S. Alexander, S. Cory, R.D. Palmiter, R.L. Brinster, The c-myc oncogene driven by immunoglobulin enhancers induces lymphoid malignancy in transgenic mice, Nature 318 (1985) 533–538, https://doi.org/10.1038/318533a0.

[26] L.A. Donehower, M. Harvey, B.L. Slagle, M.J. McArthur, C.A. Montgomery Jr., J.S. Butel, A. Bradley, Mice deficient for p53 are developmentally normal but susceptible to spontaneous tumours, Nature 356 (1992) 215–221, https://doi.org/10.1038/356215a0.

[27] S. Polakova, L. Molnarova, R.W. Hyppa, Z. Benko, I. Misova, A. Schleiffer, G.R. Smith, J. Gregan, Dbl2 regulates Rad51 and DNA joint molecule metabolism to ensure proper meiotic chromosome segregation, PLoS Genet. 12 (2016) e1006102, https://doi.org/10.1371/journal.pgen.1006102.

[28] J. Kim, G.J. Augustine, Molecular layer interneurons: key elements of cerebellar network computation and behavior, Neuroscience 462 (2021) 22–35, https://doi.org/10.1016/j.neuroscience.2020.10.008.

[29] D. Branzei, M. Foiani, Regulation of DNA repair throughout the cell cycle, Nat. Rev. Mol. Cell Biol. 9 (2008) 297–308, https://doi.org/10.1038/nrm2351.

[30] F. Yuan, J. El Hokayem, W. Zhou, Y. Zhang, FANCI protein binds to DNA and interacts with FANCD2 to recognize branched structures, J. Biol. Chem. 284 (2009) 24443–24452, https://doi.org/10.1074/jbc.M109.016006.

[31] P. Alcon, S. Shakeel, Z.A. Chen, J. Rappsilber, K.J. Patel, L.A. Passmore, FANCD2-FANCI is a clamp stabilized on DNA by monoubiquitination of FANCD2 during DNA repair, Nat. Struct. Mol. Biol. 27 (2020) 240–248, https://doi.org/10.1038/s41594-020-0380-1.

[32] P. Knipscheer, M. Raschle, A. Smogorzewska, M. Enoiu, T.V. Ho, O.D. Scharer, S.J. Elledge, J.C. Walter, The Fanconi anemia pathway promotes replication-dependent DNA interstrand cross-link repair, Science 326 (2009) 1698–1701, https://doi.org/10.1126/science.1182372.

[33] S. Houghtaling, C. Timmers, M. Noll, M.J. Finegold, S.N. Jones, M.S. Meyn, M. Grompe, Epithelial cancer in Fanconi anemia complementation group D2 (Fancd2) knockout mice, Genes Dev. 17 (2003) 2021–2035, https://doi.org/10.1101/gad.1103403.

[34] M. Koivusalo, M. Baumann, L. Uotila, Evidence for the identity of glutathione-dependent formaldehyde dehydrogenase and class III alcohol dehydrogenase, FEBS Lett. 257 (1989) 105–109, https://doi.org/10.1016/0014-5793(89)81797-1.

[35] H. Huang, M.S. Solomon, P.B. Hopkins, Formaldehyde preferentially interstrand cross-links duplex DNA through deoxyadenosine residues at the sequence 5'-d (AT), J. Am. Chem. Soc. 114 (1992) 9240–9241, https://doi.org/10.1021/ja00049a097.

[36] H. Huang, P.B. Hopkins, DNA interstrand cross-linking by formaldehyde: nucleotide sequence preference and covalent structure of the predominant cross-link formed in synthetic oligonucleotides, J. Am. Chem. Soc. 115 (1993) 9402–9408, https://doi.org/10.1021/ja00074a005.

[37] R. Yu, Y. Lai, H.J. Hartwell, B.C. Moeller, M. Doyle-Eisele, D. Kracko, W.M. Bodnar, T.B. Starr, J.A. Swenberg, Formation, accumulation, and hydrolysis of endogenous and exogenous formaldehyde-induced DNA damage, Toxicol. Sci. 146 (2015) 170–182, https://doi.org/10.1093/toxsci/kfv079.

[38] I.V. Rosado, F. Langevin, G.P. Crossan, M. Takata, K.J. Patel, Formaldehyde catabolism is essential in cells deficient for the Fanconi anemia DNA-repair pathway, Nat. Struct. Mol. Biol. 18 (2011) 1432–1434, https://doi.org/10.1038/nsmb.2173.

[39] L.B. Pontel, I.V. Rosado, G. Burgos-Barragan, J.I. Garaycoechea, R. Yu, M.J. Arends, G. Chandrasekaran, V. Broecker, W. Wei, L. Liu, et al., Endogenous formaldehyde is a hematopoietic stem cell genotoxin and metabolic carcinogen, Mol. Cell 60 (2015) 177–188, https://doi.org/10.1016/j.molcel.2015.08.020.

[40] W. Wei, B. Li, M.A. Hanes, S. Kakar, X. Chen, L. Liu, S-nitrosylation from GSNOR deficiency impairs DNA repair and promotes hepatocarcinogenesis, Sci. Transl. Med. 2 (2010) 19ra13, https://doi.org/10.1126/scitranslmed.3000328.

[41] R. Kumari, P. Jat, Mechanisms of cellular senescence: cell cycle arrest and senescence associated secretory phenotype, Front. Cell Dev. Biol. 9 (2021) 645593, https://doi.org/10.3389/fcell.2021.645593.

[42] H.C. Reinhardt, B. Schumacher, The p53 network: cellular and systemic DNA damage responses in aging and cancer, Trends Genet. 28 (2012) 128–136, https://doi.org/10.1016/j.tig.2011.12.002.

[43] D.P. Lane, Cancer. p53, guardian of the genome, Nature 358 (1992) 15–16, https://doi.org/10.1038/358015a0.

[44] X. Chen, T. Zhang, W. Su, Z. Dou, D. Zhao, X. Jin, H. Lei, J. Wang, X. Xie, B. Cheng, et al., Mutant p53 in cancer: from molecular mechanism to therapeutic modulation, Cell Death Dis. 13 (2022) 974, https://doi.org/10.1038/s41419-022-05408-1.

[45] J.F. Armstrong, M.H. Kaufman, D.J. Harrison, A.R. Clarke, High-frequency developmental abnormalities in p53-deficient mice, Curr. Biol. 5 (1995) 931–936, https://doi.org/10.1016/s0960-9822(95)00183-7.

[46] A.R.D. Delbridge, A.J. Kueh, F. Ke, N.M. Zamudio, F. El-Saafin, N. Jansz, G.Y. Wang, M. Iminitoff, T. Beck, S. Haupt, et al., Loss of p53 causes stochastic aberrant X-chromosome inactivation and female-specific neural tube defects, Cell Rep. 27 (2019) 442–454, https://doi.org/10.1016/j.celrep.2019.03.048, e445.

[47] T. Jacks, L. Remington, B.O. Williams, E.M. Schmitt, S. Halachmi, R.T. Bronson, R.A. Weinberg, Tumor spectrum analysis in p53-mutant mice, Curr. Biol. 4 (1994) 1–7, https://doi.org/10.1016/s0960-9822(00)00002-6.

[48] S.M. Lipkin, P.B. Moens, V. Wang, M. Lenzi, D. Shanmugarajah, A. Gilgeous, J. Thomas, J. Cheng, J.W. Touchman, E.D. Green, et al., Meiotic arrest and aneuploidy in MLH3-deficient mice, Nat. Genet. 31 (2002) 385–390, https://doi.org/10.1038/ng931.

[49] V.S. Jonnalagadda, T. Matsuguchi, B.P. Engelward, Interstrand crosslink-induced homologous recombination carries an increased risk of deletions and insertions, DNA Repair 4 (2005) 594–605, https://doi.org/10.1016/j.dnarep.2005.02.002.

[50] C.A. Nichols, W.J. Gibson, M.S. Brown, J.A. Kosmicki, J.P. Busanovich, H. Wei, L.M. Urbanski, N. Curimjee, A.C. Berger, G.F. Gao, et al., Loss of heterozygosity of essential genes represents a widespread class of potential cancer vulnerabilities, Nat. Commun. 11 (2020) 2517, https://doi.org/10.1038/s41467-020-16399-y.

[51] M.E. Moynahan, M. Jasin, Mitotic homologous recombination maintains genomic stability and suppresses tumorigenesis, Nat. Rev. Mol. Cell Biol. 11 (2010) 196–207, https://doi.org/10.1038/nrm2851.

[52] S.A. Hagstrom, T.P. Dryja, Mitotic recombination map of 13cen-13q14 derived from an investigation of loss of heterozygosity in retinoblastomas, Proc. Natl. Acad. Sci. U. S. A. 96 (1999) 2952–2957, https://doi.org/10.1073/pnas.96.6.2952.

[53] J.R. Ridpath, A. Nakamura, K. Tano, A.M. Luke, E. Sonoda, H. Arakawa, J.M. Buerstedde, D.A. Gillespie, J.E. Sale, M. Yamazoe, et al., Cells deficient in the FANC/BRCA pathway are hypersensitive to plasma levels of formaldehyde, Cancer Res. 67 (2007) 11117–11122, https://doi.org/10.1158/0008-5472.CAN-07-3028.

[54] T. Noda, A. Takahashi, N. Kondo, E. Mori, N. Okamoto, Y. Nakagawa, K. Ohnishi, M.Z. Zdzienicka, L.H. Thompson, T. Helleday, et al., Repair pathways independent of the Fanconi anemia nuclear core complex play a predominant role in mitigating formaldehyde-induced DNA damage, Biochem. Biophys. Res. Commun. 404 (2011) 206–210, https://doi.org/10.1016/j.bbrc.2010.11.094.

[55] G.H. Jones, F.C. Franklin, Meiotic crossing-over: obligation and interference, Cell 126 (2006) 246–248, https://doi.org/10.1016/j.cell.2006.07.010.

[56] T. Potapova, G.J. Gorbsky, The consequences of chromosome segregation errors in mitosis and meiosis, Biology 6 (2017), https://doi.org/10.3390/biology6010012.

[57] P. Singh, R. Fragoza, C.S. Blengini, T.N. Tran, G. Pannafino, N. Al-Sweel, K.J. Schimenti, K. Schindler, E.A. Alani, H. Yu, J.C. Schimenti, Human MLH1/3 variants causing aneuploidy, pregnancy loss, and premature reproductive aging, Nat. Commun. 12 (2021) 5005, https://doi.org/10.1038/s41467-021-25028-1.

[58] I. Misova, A. Pitelova, J. Budis, J. Gazdarica, T. Sedlackova, A. Jordakova, Z. Benko, M. Smondrkova, N. Mayerova, K. Pichlerova, et al., Repression of a large number of genes requires interplay between homologous recombination and HIRA, Nucleic Acids Res. 49 (2021) 1914–1934, https://doi.org/10.1093/nar/gkab027.

[59] H. Yang, H. Wang, R. Jaenisch, Generating genetically modified mice using CRISPR/Cas-mediated genome engineering, Nat. Protoc. 9 (2014) 1956–1968, https://doi.org/10.1038/nprot.2014.134.

[60] P. Pozarowski, Z. Darzynkiewicz, Analysis of cell cycle by flow cytometry, Methods Mol. Biol. 281 (2004) 301–311, https://doi.org/10.1385/1-59259-811-0:301.

[61] F. Dia, T. Strange, J. Liang, J. Hamilton, K.M. Berkowitz, Preparation of meiotic chromosome spreads from mouse spermatocytes, J. Vis. Exp. (2017), https://doi.org/10.3791/55378.
[62] J.R. Gruhn, C. Rubio, K.W. Broman, P.A. Hunt, T. Hassold, Cytological studies of human meiosis: sex-specific differences in recombination originate at, or prior to, establishment of double-strand breaks, PLoS One 8 (2013) e85075, https://doi.org/10.1371/journal.pone.0085075.
[63] M.G. Brattain, W.D. Fine, F.M. Khaled, J. Thompson, D.E. Brattain, Heterogeneity of malignant cells from a human colonic carcinoma, Cancer Res. 41 (1981) 1751–1756.
[64] J. Ponten, E. Saksela, Two established in vitro cell lines from human mesenchymal tumours, Int. J. Cancer 2 (1967) 434–447, https://doi.org/10.1002/ijc.2910020505.
[65] L. Montoliu, Mendel: a simple excel workbook to compare the observed and expected distributions of genotypes/phenotypes in transgenic and knockout mouse crosses involving up to three unlinked loci by means of a chi2 test, Transgenic Res. 21 (2012) 677–681, https://doi.org/10.1007/s11248-011-9544-4.